

Ultrafast Photoconductivity of Graphene Nanoribbons and Carbon Nanotubes

Søren A. Jensen,^{†,‡} Ronald Ulbricht,[†] Akimitsu Narita,[‡] Xinliang Feng,[‡] Klaus Müllen,[‡] Tobias Hertel,^{||} Dmitry Turchinovich,^{‡,§} and Mischa Bonn^{*,‡}

[†]FOM Institute AMOLF, Science Park 104, 1098 XG Amsterdam, The Netherlands

[‡]Max Planck Institute for Polymer Research, Ackermannweg 10, 55128 Mainz, Germany

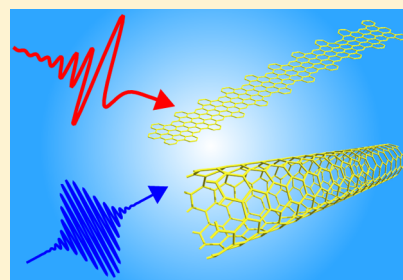
[§]DTU Fotonik, Technical University of Denmark, Ørsteds Plads 343, 2800 Lyngby, Denmark

^{||}Institute of Physical and Theoretical Chemistry, Julius-Maximilian University, 97070 Würzburg, Germany

Supporting Information

ABSTRACT: We present a comparative study of the ultrafast photoconductivity in two different forms of one-dimensional (1D) quantum-confined graphene nanostructures: structurally well-defined semiconducting graphene nanoribbons (GNRs) fabricated by a “bottom-up” chemical synthesis approach and semiconducting carbon nanotubes (CNTs) with a similar bandgap energy. Transient photoconductivities of both materials were measured using time-resolved terahertz spectroscopy, allowing for contact-free measurements of complex-valued photoconductivity spectra with subpicosecond time-resolution. We show that, while the THz photoresponse seems very different for the two systems, a single model of free carriers experiencing backscattering when moving along the long axis of the CNTs or GNRs provides a quantitative description of both sets of results, revealing significantly longer carrier scattering times for CNTs (ca. 150 fs) than for GNRs (ca. 30 fs) and in turn higher carrier mobilities. This difference can be explained by differences in band structures and phonon scattering and the greater structural rigidity of CNTs as compared to GNRs, minimizing the influence of bending and/or torsional defects on the electron transport.

KEYWORDS: Graphene nanoribbon, carbon nanotube, THz time-domain spectroscopy, photoconductivity, charge carrier dynamics



Graphene is a stable form of graphite with a thicknesses of just a single atomic layer.¹ Charge carriers in this two-dimensional semimetallic material are described as massless relativistic Dirac fermions,^{2,3} with reported charge carrier mobilities as high as $200\,000\text{ cm}^2\text{ V}^{-1}\text{ s}^{-1}$.⁴ However, owing to its vanishing bandgap, graphene is unsuitable for many electronic applications, such as field effect transistors (FETs) and photovoltaic devices.⁵

To induce a bandgap in graphene, quantum confinement can be employed.^{6,7} Two types of one-dimensional graphene-based structures have been established, achieving carrier confinement in the lateral dimension: carbon nanotubes (CNTs) and flat graphene nanoribbons (GNRs) with nanometer-scale widths. In both CNTs and GNRs, the bandgap is associated with electron motion along the shorter dimension of the system: circular motion along the circumference of the CNT and in-plane motion across the width of the GNR.⁵ Both GNRs and CNTs are considered vital to the emerging field of carbon nanoelectronics.⁵ Already, entire logic circuits based on single CNTs have been realized,⁸ as well as CNT^{9–12} and GNR-based¹³ FETs. CNT based photovoltaic devices have been demonstrated,^{14,15} and calculations predict that narrow GNRs with well-defined edge structures can exhibit bandgaps corresponding to visible photon energies and a band alignment with the common electron acceptor C_{60} favorable for

photovoltaic applications.¹⁶ The nature of photogenerated charges (excitons or free charges) and the charge carrier mobility is crucial for the performance of such devices.

Surprisingly, despite their very similar chemical and electronic structure—CNTs are essentially “rolled up” GNRs^{17–19}—ultrafast photoconductivity measurements performed on both CNTs^{20,21} and GNRs²² have led to varying conclusions on the primary photoproducts. Xu et al.²¹ found that the photoresponse of isolated CNTs was dominated by electrons and holes tightly bound in excitons. These neutral quasi-particles cannot be accelerated by applied electric fields and therefore do not contribute to long-range conductivity. Beard et al.²⁰ reported the initial generation of free carriers in CNT films, unbound, but obstructed in their motion by the corrugated potential energy landscape within the conductor. Similarly, for GNRs the presence of short-lived free charge carriers has been concluded.²²

Here, we present a unified view of the photogenerated species in structurally well-defined GNRs and CNTs through the transient photoconductivity responses obtained by optical pump–THz probe spectroscopy. Using this measurement

Received: August 8, 2013

Revised: September 23, 2013

Published: October 4, 2013

technique and appropriate modeling, the presence of excitons and (quasi) free charge carriers can be distinguished.^{23,24} We show that one model of restricted free charge carrier motion is capable of quantitatively reproducing the results for both GNRs and CNTs, although the photoconductive responses appear different.

We quantify the ultrafast photoconductive response using THz time-resolved spectroscopy (TRTS). TRTS employs a single, freely propagating picosecond (ps) cycle of the electric field for contact-free probing of photogenerated charge carriers.²³ The THz electric field transmitted through the (photoexcited) sample is detected in time, and therefore, via Fourier transform, both phase and amplitude spectral information is readily accessible within the full spectral bandwidth of the THz probe. From this information the real and imaginary parts of the complex frequency-dependent photoconductivity $\sigma(\omega)$ are extracted. By varying the delay between the optical pump and the THz probe, the time evolution of the photoinduced conductivity can be mapped out with subpicosecond time resolution. Details on the TRTS measurements employed here and the extraction of $\sigma(\omega)$ are presented in the Supporting Information.

Structurally well-defined and narrow (1.1 nm) GNRs with an average length of about 600 nm and an optical bandgap of 1.88 eV were chemically synthesized as described in ref 22; see Figure 1. The advantage of this newly developed chemical

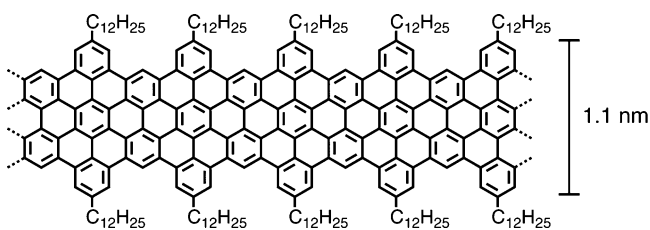


Figure 1. Chemical structure of the GNRs investigated. Quantum confinement in the lateral dimension induces a bandgap of 1.88 eV.

“bottom up” synthesis approach is that it allows for the fabrication of GNRs with sub-5 nm widths, giving rise to bandgap energies corresponding to visible excitation wavelengths, as well as well-defined edge structures.^{25,26} The alkyl ($C_{12}H_{25}$) chains on the peripheral positions are required to render the GNRs dispersible in organic solvents. Our measurements were performed on two types of GNR samples: (i) GNRs dispersed in 1,2,4-trichlorobenzene (TCB) and (ii) GNRs dropcast on a fused silica substrate from dispersion. The TCB solvent is transparent at both optical and THz frequencies.

Two analogous types of CNT samples were prepared: (i) individual CNTs dispersed in an organic gel phase to achieve separation between the CNTs, similar to the environment of the GNRs dispersed in TCB, and (ii) a film consisting of CNT aggregates similar to the dropcast GNR film. Prior to processing, CNTs were diameter-sorted by density gradient ultracentrifugation. Approximately 97% of the CNTs were semiconducting, and of those 97% at least 90% were the semiconducting (6,5)-tubes which have a diameter of 0.76 nm. The average tube length was approximately 260 nm. In the film, the aggregates were several micrometers long and interlocking with each other.

In the TRTS measurements, carriers are photoexcited with near- or above bandgap photon energies, and their conductive

response is probed on subpicosecond time scales. This way the dynamics of photogenerated carriers in both semiconducting and metallic CNTs are probed, but the response of the semiconducting tubes dominates because of their abundance.

Figure 2 shows the photoconductivity σ of the two GNR samples, scaled to the absorbed photon density N , as a function of pump–probe delay (Figure 2a,c) or probe frequency (Figure 2b,d). The dynamics of real and imaginary conductivity following excitation (Figure 2a,c) were acquired in a frequency-integrated fashion by measuring the attenuation and the time-shift, respectively, of the THz waveform. The frequency-resolved complex-valued conductivity spectra were measured at a pump delay of ~ 300 fs after photoexcitation (corresponding to the highest value of frequency-integrated conductivities in Figure 2a,c). The GNRs dispersed in TCB show a conductivity rising just after excitation and then decaying with a characteristic exponential lifetime close to 1 ps (Figure 2a), with an additional slower decay component apparent at later times. As the initial photoconductivity decays, the magnitude of the imaginary conductivity increases relative to the real conductivity. Purely imaginary conductivity is evidence of the presence of a restoring force in the electron motion, which indicates bound charges in the form of excitons.²⁷ Hence the observation of large initial real conductivity and the subsequent relative increase in imaginary conductivity is consistent with initial excitation of free carriers which quickly form excitons on time scale close to 1 ps. Efficient exciton formation typically occurs in systems with strong quantum confinement²⁸ and weak screening²⁹ ($\epsilon = 2.24$ for TCB), which both lead to an increase in exciton binding energy.

In the frequency-resolved conductivity spectra of the GNRs in dispersion, positive real- and negative imaginary conductivity is observed, both increasing in magnitude with probe frequency, as shown in Figure 2b. This behavior is qualitatively similar to results obtained on semiconducting polymers, such as poly(2-methoxy-5-(2-ethyl-hexyloxy)-*p*-phenylene vinylene) (MEH-PPV).²⁹ However, the magnitude of the conductivity scaled to the excitation density is almost an order of magnitude larger for the GNRs compared to MEH-PPV in solution.²⁹ For MEH-PPV it was shown that the charge carrier mobility is limited by torsional and conjugation irregularities along the polymer backbone.²⁹ Thus the larger photoconductive response of GNRs is likely the result of the relatively rigid structure of the GNRs as compared to MEH-PPV, causing less torsional and conjugation irregularities as compared to a polymer backbone.

The conductivity experiments on GNRs in dispersion were performed at six different (absorbed) pump intensities between 1.2×10^{18} photons/m² and 1.3×10^{19} photons/m². A similar spectral shape and decay dynamics of the conductivity was observed at all pump intensities, and the conductivity magnitude was found to scale almost linearly with pump intensity (data not shown). Experiments on GNRs in the different solvent 1,2-dichlorobenzene revealed no dependence of the observed response on solvent. Preliminary experiments on slightly wider GNRs also revealed a very similar photoconductive response.

As for the dropcast GNR film, the spectrally integrated real-valued conductivity decays with a characteristic lifetime of 0.6 ps, as shown in Figure 2c, faster than for GNRs in dispersion. Yet another difference from the results on the GNR dispersion is that the complex conductivity spectrum (see Figure 2d) is

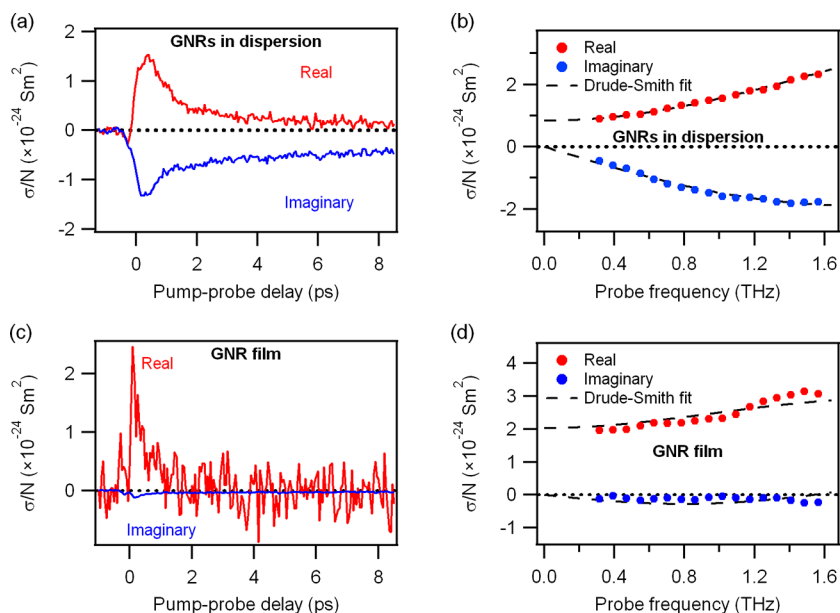


Figure 2. THz photoconductivity of GNRs dispersed in 1,2,4-trichlorobenzene (a,b) and dropcast on fused silica (c,d), excited by 400 nm pulses with a sheet excitation density of 1.3×10^{19} photons/m² for the dispersion and of 2.1×10^{18} photons/m² for the film. The conductivity is scaled to the density N of absorbed photons. Graphs a and c show pump–probe delay scans of the frequency averaged conductivity, and graphs b and d show the complex frequency-resolved conductivity measured 300 fs after photoexcitation, at the peak of photoconductivity. The peak magnitudes in plots a and c are scaled to the frequency averaged conductivities of plots b and d, respectively. Lines in b and d show Drude–Smith fits explained in the main text.

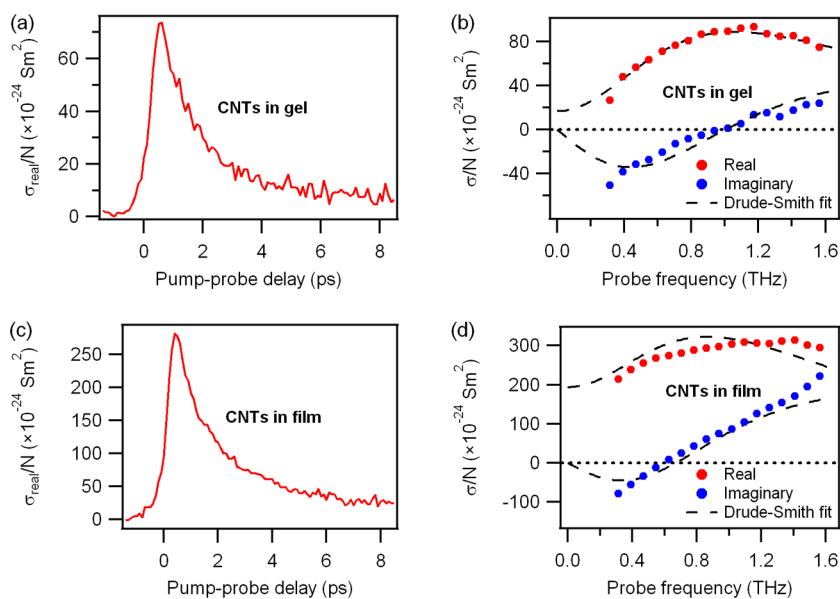


Figure 3. THz photoconductivity of CNTs separated in gel a and b and film of agglomerated CNTs c and d excited by 800 nm pulses with a sheet excitation density of 2.2×10^{17} photons/m², scaled to absorbed photon density N . Parts a and c show pump–probe delay scans of the frequency-averaged real conductivity, and b and d show the complex probe frequency-resolved conductivity measured just after photoexcitation, where the photoconductivity is highest. The peak magnitudes in plots a and c are scaled to the frequency averaged conductivities of plots b and d, respectively. Lines in b and d show Drude–Smith fits.

predominantly real-valued. This suggests that also in the film the short-time photoconductivity stems mainly from free carriers without substantial localization and that less excitons are formed during the relaxation process as compared to the dispersed GNRs. We note here that morphological inhomogeneities in the dropcast film give rise to uncertainty in the extracted parameters, particularly the independently measured value of N .

Figure 3 shows the results of optical pump–THz probe spectroscopy on the second type of graphene nanostructures investigated in this work, the CNTs. Similar to GNRs, measurements were performed on dispersed CNTs, in this case in a gel matrix, and on CNTs in a dropcast film. In both cases the decay of the real conductivity with pump–probe delay revealed a lifetime close to 1.7 ps (Figure 3a,c). Quantitatively, the CNT conductivities normalized to the pump intensity are at least 1 order of magnitude larger than for GNRs. Even higher

values for the scaled conductivity were observed when going to lower excitation intensities or higher pump energies (data not shown). Qualitatively, the spectral shape of the frequency-resolved complex conductivities are similar for both CNT samples studied, but distinctly different from that of GNRs. Particularly, the imaginary component is negative at low frequencies but becomes positive at frequencies higher than ~ 1 THz. At the same zero-crossing frequency of 1 THz, the real conductivity peaks for the gel-dispersed sample. A similar behavior has previously been observed by Beard et al. on an agglomerated film of mainly semiconducting CNTs²⁰ and by Xu et al.²¹ for isolated CNTs. Beard et al.²⁰ attributed the behavior to a combination of quasi-free charge carriers and charge carriers bound in excitons. Xu et al.²¹ interpreted the response as purely excitonic. However, it has been shown³⁰ that the energy spacing between the ground state and the first excited state of the exciton for a (6,5) single wall CNT is 310 meV, corresponding to 75 THz, far outside the frequency window of our THz spectroscopy experiment. Additionally, the characteristic decay time of 1.7 ps for the real conductivity in both our CNT samples is considerably lower than the photoluminescence lifetimes of 9–15 ps reported for the first excitonic state in colloidal suspended (6,5) CNTs.³¹

Moreover, an excitonic response is not consistent with the results obtained from the GNR samples. There is no reason to assume that the primary photoproduct would be very different in these two one-dimensional graphene nanostructures. We therefore expect the THz-range photoinduced conductivity of CNTs *immediately after excitation* to be dominated by free carriers rather than excitons, similar to the behavior of semiconducting polymers reported previously. Hence, we describe the observed responses of both GNRs and CNTs with a model that has successfully been used to describe complex conductivities in semiconducting polymers.^{32,33} This is the Drude–Smith (DS) model, describing the conductivity of free carriers in a medium with preferential charge carrier backscattering:³⁴

$$\sigma_{\text{DS}} = \frac{\epsilon_0 \omega_p^2 \tau}{1 - i\tau\omega} \times \left(1 + \frac{c}{1 - i\omega\tau} \right) \quad (1)$$

Here ϵ_0 is the vacuum permittivity, ω_p is the plasma frequency, τ is the average scattering time, and c denotes the probability that a carrier maintains its velocity in a scattering event: $c = 0$ describes fully momentum randomizing scattering (and thus the model reduces to a classical Drude conductivity model), and $c = -1$ describes complete preferential backscattering. The plasma frequency is related to the density of excited charge carriers N_{ex} by

$$\omega_p^2 = \frac{e^2 N_{\text{ex}}}{\epsilon_0 m^*} \quad (2)$$

where e is the elemental charge and m^* is the carrier effective mass.

An important point should be made here: in THz photoconductivity measurements on 1D structures, only the electronic transport in the linearly polarized THz probe field *along* the long axis of the GNR or CNT is probed. As the spatial orientation of the 1D graphene nanostructures in these measurements is random, one is always probing the spatial-orientation-averaged conductivity of the whole ensemble of the GNRs or CNTs.

Assuming $c = -1$ for conductors oriented perpendicular to the THz probe field polarization, and $c = 0$ for the ones perfectly parallel to the THz field, an ensemble-average value of c can be calculated (see Supporting Information) to be $-\pi/4 \approx -0.79$ for 1D conductors oriented randomly in three dimensions (relevant for the dispersed GNRs or CNTs samples), and $-2/\pi \approx -0.64$ for conductors oriented randomly in a two-dimensional plane containing the THz polarization (at least partially relevant for GNRs or CNTs in dropcast films). As will be shown below, the c values extracted from our measurements are fairly close to these values, which are simply dictated by the (random) orientation of tubes and ribbons in the experiment. The key parameter of the DS model, describing the intrinsic conductivity of the GNRs and CNTs, is the carrier momentum scattering time τ , which determines the carrier mobility.

For the GNRs and CNTs measured in this work, eq 1 is valid only when the conductivity is probed on length scales shorter than the actual length of the nanostructure, so that the effects of the ends of the conducting molecules can be neglected. This condition is met by the high, terahertz-range probe frequencies used in our experiments.

By fitting the frequency-resolved conductivities of the GNRs (Figure 2b,d) to eq 1, the c parameters were found to be -0.92 for the GNRs in dispersion and -0.79 for the GNR films (Table 1), in reasonable agreement with the c values predicted

Table 1. Fit Parameters from the Probe Frequency-Dependent GNR Data and CNT Conductivity Fitted to the Drude–Smith Model, eq 1^a

	c	τ (fs)	QY (%)
GNR dispersion	-0.92 ± 0.01	30 ± 3	3 ± 1
GNR film	-0.79 ± 0.07	35 ± 20	4 ± 3
CNTs in gel	-0.90 ± 0.02	170 ± 50	15 ± 10
CNT film	-0.72 ± 0.05	150 ± 15	27 ± 10

^aAn effective mass of $1.7m_e$ was assumed for carriers in GNRs^{32,33} and $1.0m_e$ for carriers in CNTs.²⁰ Data was measured at various excitation densities. In the case of the GNR film, two separate films made from the same GNRs were prepared and measured, and in the case of the CNTs, two excitation wavelengths, 800 and 400 nm, were used. The numbers provided are average values and standard deviations.

above for randomly oriented one-dimensional Drude conductors in, respectively, three and two dimensions. We obtain a mean carrier momentum scattering time of $\tau = 30$ fs for the dispersed GNRs measured at various excitation densities, and $\tau = 35$ fs for two separately prepared GNR film excited with 2.1×10^{18} photons/m² and 3.5×10^{18} photons/m², respectively; see Table 1. These values are very similar to the values of 30 fs – 43 fs obtained for a film of regioregular poly(3-hexylthiophene) (P3HT) by Cunningham and Hayden.³² From the DS fits we could extract the plasma frequencies, and assuming a free carrier effective mass of $1.7m_e$ ^{32,33} the density of excited carriers N_{ex} could be determined. Comparing the carrier density N_{ex} to the density of absorbed photons N , a quantum yield (QY) of free carrier excitation of roughly 3–4% is found for both the GNRs in dispersion and the GNRs in the dropcast films. These results are consistent with previous reports of optical pump–THz probe measurements on films of the conducting polymer P3HT.^{32,33} We note that our frequency-dependent conductivity data for the GNRs cannot be adequately fitted with a Lorentzian model, describing the

electronic transition in a bound complex, such as a $1s-2p$ intraexcitonic transition.³⁵

As seen in Figure 3b,d and Table 1, the DS model also describes the photoconductive response of the CNTs very well. Since the GNRs of dimensions similar to the CNTs studied here show free charge carrier behavior right after photoexcitation, and given the discussion of the CNT results above, we conclude that the dominant photogenerated species in the CNTs right after photoexcitation are free carriers experiencing preferential backscattering as described by the Drude–Smith model, with the parameters summarized in Table 1.

It should be noted that, even though free charge carriers were found to dominate the photoconductive response of both GNRs and CNTs, this does not mean that these are the only species present right after excitation. Specifically, excitons are expected to be generated as well. Excitons do not contribute to the real conductivity in the probed spectral range but can contribute by a small amount to the imaginary part of the conductivity²⁷ and as such may contribute to slight deviations between the data and the Drude–Smith fits seen in Figure 3.

Since the Drude–Smith model is found to adequately describe the frequency-resolved photoconductivity of both GNRs and CNTs, we can now compare the model parameters for both types of graphene nanostructures. We find c values of -0.90 for the CNTs suspended in gel and -0.72 for the film, again consistent with the predicted c values and the values obtained for the GNRs. Interestingly, we find a significantly longer electron momentum scattering time for the CNT samples (~ 160 fs) than for the GNRs (~ 30 fs), consistent with previous theoretical efforts taking into account the band structures and the effects of phonon scattering.³⁶ Indeed, in ref 36 it was predicted that the mobility in CNTs is larger than for GNRs for a given bandgap and that the mobility increases with decreasing bandgap. The difference in scattering times can be understood by noting that the bandgap for a CNT with a given circumference is lower than that of a GNR with the same width. As the (6,5) tubes studied here have a bandgap of roughly 1.5 eV, that is, lower than the 1.88 eV bandgap of the GNRs, it is to be expected that the mobilities in the CNT system are higher than for the GNRs. For a dispersion or a dropcast layer of GNRs, bends and kinks will be present in the GNRs, leading to increased electron backscattering along the nanoribbon. The significantly more rigid structure of the CNTs is expected to reduce this effect, explaining the longer carrier electron momentum scattering times in CNTs as compared to GNRs. Additionally, as the GNR edges are terminated with flexible alkyl chains, see Figure 1, coupling to vibrational modes of these chains may also contribute to the observed enhanced momentum scattering for carrier motion along the GNR.

In conclusion, although the complex-valued THz photoconductivity spectra of GNRs and CNTs appear to be different both in shape and magnitude, all observations made here can be explained by the same mechanism. The response of GNRs clearly resembles the conductivity of free charge carriers with preferential backscattering, as described by the Drude–Smith model, eq 1, very similar to semiconducting polymers.^{32,33} The key reason for this measured preferential backscattering is the random orientation of 1D conductors (which also includes randomly bent GNRs and CNTs). The electron momentum scattering times, extracted using the Drude–Smith model, reflect the microscopic electron transport within the studied graphene nanostructures. The photoconductivity of CNTs can be described by the same model as the GNRs, indicating free

charge carriers in the CNTs as well, but using a longer electron scattering time (and hence higher electron mobility), which indicates less electron scattering events. The latter originates from both differences in band structure and carrier-phonon interactions, as well as the larger structural rigidity of a CNT as compared to a GNR, which minimizes the influence of bending and/or torsional defects on electron transport along the long dimension of the conductor. The presence of free photoexcited carriers in CNTs and GNRs, as opposed to neutrally charged excitons, is a positive result for applications in carbon and hybrid nanoelectronics.⁵ Our findings of longer scattering times and higher free carrier generation quantum efficiency in CNTs as compared to GNRs suggest that CNT-based (opto)-electronic devices will likely be more efficient than GNR-based ones.

■ ASSOCIATED CONTENT

📄 Supporting Information

Experimental details on time-resolved THz spectroscopy and the extraction of the THz photoconductivity from the measured data. Calculation of the Drude–Smith c parameter for ideal one-dimensional conductors oriented uniformly in two and three dimensions. This material is available free of charge via the Internet at <http://pubs.acs.org>.

■ AUTHOR INFORMATION

Corresponding Author

*E-mail: bonn@mpip-mainz.mpg.de.

Present Address

R.U.: Division of Applied Physics, Graduate School of Engineering, Hokkaido University, Sapporo, Japan.

Notes

The authors declare no competing financial interest.

■ ACKNOWLEDGMENTS

This work has been financially supported by the Nederlandse Organisatie voor Wetenschappelijk Onderzoek (NWO) within the research program “Stichting voor Fundamenteel Onderzoek der Materie (FOM)”, ERC grant NANOGRAPH, DFG Priority Program SPP 1459, EU Projects GENIUS and UPGRADE, Max Planck Society, Danish Council for Independent Research—Technology and Production Sciences (FTP project ALFIE), and EU Career Integration Grant 334324 LIGHTER.

■ REFERENCES

- (1) Novoselov, K. S.; Geim, A. K.; Morozov, S. V.; Jiang, D.; Zhang, Y.; Dubonos, S. V.; Grigorieva, I. V.; Firsov, A. A. *Science* **2004**, *306* (5696), 666–669.
- (2) Novoselov, K. S.; Geim, A. K.; Morozov, S. V.; Jiang, D.; Katsnelson, M. I.; Grigorieva, I. V.; Dubonos, S. V.; Firsov, A. A. *Nature* **2005**, *438* (7065), 197–200.
- (3) Zhang, Y. B.; Tan, Y. W.; Stormer, H. L.; Kim, P. *Nature* **2005**, *438* (7065), 201–204.
- (4) Bolotin, K. I.; Sikes, K. J.; Jiang, Z.; Klima, M.; Fudenberg, G.; Hone, J.; Kim, P.; Stormer, H. L. *Solid State Commun.* **2008**, *146* (9–10), 351–355.
- (5) Avouris, P.; Chen, Z. H.; Perebeinos, V. *Nat. Nanotechnol.* **2007**, *2* (10), 605–615.
- (6) Castro Neto, A. H.; Guinea, F.; Peres, N. M. R.; Novoselov, K. S.; Geim, A. K. *Rev. Mod. Phys.* **2009**, *81* (1), 109–162.
- (7) Terrones, M.; Botello-Mendez, A. R.; Campos-Delgado, J.; Lopez-Urias, F.; Vega-Cantu, Y. I.; Rodriguez-Macias, F. J.; Elias, A. L.; Munoz-Sandoval, E.; Cano-Marquez, A. G.; Charlier, J. C.; Terrones, H. *Nano Today* **2010**, *5* (4), 351–372.

- (8) Chen, Z. H.; Appenzeller, J.; Lin, Y. M.; Sippel-Oakley, J.; Rinzler, A. G.; Tang, J. Y.; Wind, S. J.; Solomon, P. M.; Avouris, P. *Science* **2006**, *311* (5768), 1735–1735.
- (9) Misewich, J. A.; Martel, R.; Avouris, P.; Tsang, J. C.; Heinze, S.; Tersoff, J. *Science* **2003**, *300* (5620), 783–786.
- (10) Chen, J.; Perebeinos, V.; Freitag, M.; Tsang, J.; Fu, Q.; Liu, J.; Avouris, P. *Science* **2005**, *310* (5751), 1171–1174.
- (11) Freitag, M.; Martin, Y.; Misewich, J. A.; Martel, R.; Avouris, P. *Nano Lett.* **2003**, *3* (8), 1067–1071.
- (12) Qiu, X. H.; Freitag, M.; Perebeinos, V.; Avouris, P. *Nano Lett.* **2005**, *5* (4), 749–752.
- (13) Chen, Z. H.; Lin, Y. M.; Rooks, M. J.; Avouris, P. *Physica E* **2007**, *40* (2), 228–232.
- (14) Ramuz, M. P.; Vosgueritchian, M.; Wei, P.; Wang, C. G.; Gao, Y. L.; Wu, Y. P.; Chen, Y. S.; Bao, Z. N. *ACS Nano* **2012**, *6* (11), 10384–10395.
- (15) Jung, Y.; Li, X. K.; Rajan, N. K.; Taylor, A. D.; Reed, M. A. *Nano Lett.* **2013**, *13* (1), 95–99.
- (16) Osella, S.; Narita, A.; Schwab, M. G.; Hernandez, Y.; Feng, X. L.; Müllen, K.; Beljonne, D. *ACS Nano* **2012**, *6* (6), 5539–5548.
- (17) Iijima, S. *Nature* **1991**, *354* (6348), 56–58.
- (18) Iijima, S.; Ichihashi, T. *Nature* **1993**, *364* (6439), 737–737.
- (19) Bethune, D. S.; Kiang, C. H.; Devries, M. S.; Gorman, G.; Savoy, R.; Vazquez, J.; Beyers, R. *Nature* **1993**, *363* (6430), 605–607.
- (20) Beard, M. C.; Blackburn, J. L.; Heben, M. J. *Nano Lett.* **2008**, *8* (12), 4238–4242.
- (21) Xu, X. L.; Chuang, K.; Nicholas, R. J.; Johnston, M. B.; Herz, L. M. *J. Phys. Chem. C* **2009**, *113* (42), 18106–18109.
- (22) Narita, A.; Feng, X.; Hernandez, Y.; Jensen, S. A.; Bonn, M.; Yang, H.; Verzhbitskiy, I. A.; Casiraghi, C.; Hansen, M. R.; Koch, A. H. R.; Fytas, G.; Ivasenko, O.; Li, B.; Mali, K. S.; Balandina, T.; Sankarapillai, M.; De Feyter, S.; Müllen, K. *Nat. Chem.* **2013**, submitted.
- (23) Ulbricht, R.; Hendry, E.; Shan, J.; Heinz, T. F.; Bonn, M. *Rev. Mod. Phys.* **2011**, *83* (2), 543–586.
- (24) Lloyd-Hughes, J.; Jeon, T. I. *J. Infrared, Millim., Terahertz Waves* **2012**, *33* (9), 871–925.
- (25) Schwab, M. G.; Narita, A.; Hernandez, Y.; Balandina, T.; Mali, K. S.; De Feyter, S.; Feng, X. L.; Müllen, K. *J. Am. Chem. Soc.* **2012**, *134* (44), 18169–18172.
- (26) Chen, L.; Hernandez, Y.; Feng, X. L.; Müllen, K. *Angew. Chem., Int. Ed.* **2012**, *51* (31), 7640–7654.
- (27) Wang, F.; Shan, J.; Islam, M. A.; Herman, I. P.; Bonn, M.; Heinz, T. F. *Nat. Mater.* **2006**, *5* (11), 861–864.
- (28) Ando, T. *J. Phys. Soc. Jpn.* **1997**, *66* (4), 1066–1073.
- (29) Hendry, E.; Koeberg, M.; Schins, J. M.; Nienhuys, H. K.; Sundstrom, V.; Siebbeles, L. D. A.; Bonn, M. *Phys. Rev. B* **2005**, *71* (12), 125201.
- (30) Wang, F.; Dukovic, G.; Brus, L. E.; Heinz, T. F. *Science* **2005**, *308* (5723), 838–841.
- (31) Hertel, T.; Himmelein, S.; Ackermann, T.; Stich, D.; Crochet, J. *ACS Nano* **2010**, *4* (12), 7161–7168.
- (32) Cunningham, P. D.; Hayden, L. M. *J. Phys. Chem. C* **2008**, *112* (21), 7928–7935.
- (33) Ai, X.; Beard, M. C.; Knutsen, K. P.; Shaheen, S. E.; Rumbles, G.; Ellingson, R. J. *J. Phys. Chem. B* **2006**, *110* (50), 25462–25471.
- (34) Smith, N. V. *Phys. Rev. B* **2001**, *64* (15), 155106.
- (35) Kaindl, R. A.; Carnahan, M. A.; Hagele, D.; Lovenich, R.; Chemla, D. S. *Nature* **2003**, *423* (6941), 734–738.
- (36) Obradovic, B.; Kotlyar, R.; Heinz, F.; Matagne, P.; Rakshit, T.; Giles, M. D.; Stettler, M. A.; Nikonov, D. E. *Appl. Phys. Lett.* **2006**, *88* (14), 142102.